

Visualization of the type III secretion mediated *Salmonella*–host cell interface using cryo-electron tomography

Donghyun Park^{1,2}, Maria Lara-Tejero¹, M Neal Waxham³, Wenwei Li^{1,2}, Bo Hu^{4,5}, Jorge E Galán¹, Jun Liu^{1,2,4*}

¹Department of Microbial Pathogenesis, Yale University School of Medicine, New Haven, United States; ²Microbial Sciences Institute, Yale University School of Medicine, New Haven, United States; ³Department of Neurobiology and Anatomy, McGovern Medical School, The University of Texas Health Science Center at Houston, Texas, United States; ⁴Department of Microbiology and Molecular Genetics, McGovern Medical School, The University of Texas Health Science Center at Houston, Texas, United States; ⁵Department of Pathology and Laboratory Medicine, McGovern Medical School, The University of Texas Health Science Center at Houston, Texas, United States

Abstract Many important gram-negative bacterial pathogens use highly sophisticated type III protein secretion systems (T3SSs) to establish complex host-pathogen interactions. Bacterial-host cell contact triggers the activation of the T3SS and the subsequent insertion of a translocon pore into the target cell membrane, which serves as a conduit for the passage of effector proteins. Therefore the initial interaction between T3SS-bearing bacteria and host cells is the critical step in the deployment of the protein secretion machine, yet this process remains poorly understood. Here, we use high-throughput cryo-electron tomography (cryo-ET) to visualize the T3SS-mediated *Salmonella*-host cell interface. Our analysis reveals the intact translocon at an unprecedented level of resolution, its deployment in the host cell membrane, and the establishment of an intimate association between the bacteria and the target cells, which is essential for effector translocation. Our studies provide critical data supporting the long postulated direct injection model for effector translocation.

DOI: <https://doi.org/10.7554/eLife.39514.001>

*For correspondence:

jliu@yale.edu

Competing interests: The authors declare that no competing interests exist.

Funding: See page 13

Received: 25 June 2018

Accepted: 24 September 2018

Published: 03 October 2018

Reviewing editor: Kim Orth, Howard Hughes Medical Institute, University of Texas Southwestern Medical Center, United States

© Copyright Park et al. This article is distributed under the terms of the [Creative Commons Attribution License](https://creativecommons.org/licenses/by/4.0/), which permits unrestricted use and redistribution provided that the original author and source are credited.

Introduction

Type III secretion systems (T3SSs) are widely utilized by many pathogenic or symbiotic Gram-negative bacteria to directly inject bacterially encoded effector proteins into eukaryotic host cells (Deng et al., 2017; Galán et al., 2014; Notti and Stebbins, 2016). The central element of the T3SS is the injectisome, a multi-protein machine that mediates the selection and translocation of the effectors destined to travel this delivery pathway. The injectisome is highly conserved, both structurally and functionally, across different bacterial species including important pathogens such as *Salmonella*, *Yersinia*, *Shigella*, *Pseudomonas* and *Chlamydia* species. It consists of defined substructures such as the needle complex, the export apparatus, and the cytoplasmic sorting platform (Galán et al., 2014; Hu et al., 2017; Loquet et al., 2012; Schraidt and Marlovits, 2011; Worrall et al., 2016). The needle complex is composed of a membrane-anchored base, a protruding needle filament, and a tip complex at the distal end of the needle (Kubori et al., 1998; Schraidt et al., 2010; Schraidt and Marlovits, 2011; Worrall et al., 2016). The export apparatus, which is formed by several inner membrane proteins, functions as the conduit for substrate

translocation across the bacterial inner membrane (*Dietsche et al., 2016*). The sorting platform is a large cytoplasmic multiple-protein complex that orderly selects and delivers the substrates to the export apparatus (*Lara-Tejero et al., 2011*).

In many bacterial species the activity of these protein injection machines is stimulated upon contact with the target eukaryotic cell membrane, a process thought to be mediated by the tip complex (*Barta et al., 2012; Blocker et al., 2008; Deane et al., 2006; Ménard et al., 1994; Zierler and Galán, 1995*). Host cell contact triggers a cascade of poorly understood events that lead to the deployment of the protein translocases onto the host cell membrane where they form a protein channel that mediates the passage of the effector proteins. In the case of the *Salmonella enterica* serovar Typhimurium (*S. Typhimurium*) T3SS encoded within its pathogenicity island 1, the protein translocases are SipB and SipC, which through a process that requires the tip protein SipD, are inserted in the host-cell membrane to form the translocon channel (*Collazo and Galán, 1997*). Deployment of the translocon also results in the intimate association of the bacteria and the host cell, which is orchestrated by the protein translocases themselves (*Lara-Tejero and Galán, 2009; Misselwitz et al., 2011*). Despite the critical role of the translocases in intimate attachment and effector translocation, little is known about their structural organization when deployed in the host cell membrane, and previous attempts to visualize them did not provide distinct structural details. This paucity of information is due at least in part to the intrinsic difficulties of imaging bacteria/host cell interactions at high resolution. Here, we used bacterial minicells and cultured mammalian cells combined with high-throughput cryo-ET to study the initial interaction between *S. Typhimurium* and host cells. This experimental system allowed the visualization of the intact translocon deployed in the host cell membrane, in contact with the tip-complex of the T3SS injectisome, at unprecedented resolution. This study provides new insights into the initial events of the T3SS-mediated bacteria-host cell interactions and highlights the potential of cryo-ET as a valuable tool for investigating the host cell-pathogen interface.

Results

In situ structures of the T3SS injectisome in the presence or absence of protein translocases

An intrinsic property of many T3SSs is that their activity is stimulated by contact with the target host cell membrane (*Ménard et al., 1994; Zierler and Galán, 1995*). This interaction results not only in the stimulation of secretion but also in the deployment of the protein translocases in the host cell membrane, a poorly understood process that is orchestrated by the tip complex of the injectisome's needle filament. In the case of the *S. Typhimurium* SPI-1 T3SS the tip complex is thought to be composed of a single protein, SipD, which organizes as a pentamer at the tip of the needle filament (*Rathinavelan et al., 2014*). However, it has been previously proposed that in *Shigella* spp., in addition to IpaD, a homolog of SipD, the tip complex also contains IpaB, a homolog of SipB (*Cheung et al., 2015*). To get insight into the structural organization of the tip complex prior to bacterial contact with cultured cells, we compared the in situ structures of fully assembled injectisomes from minicells obtained from wild-type, $\Delta sipB$, and $\Delta sipD$ *S. Typhimurium* strains (**Figure 1A–D, Table 1**). We found that injectisomes from wild-type or the $\Delta sipB$ strains were indistinguishable from one another. In contrast, injectisomes from a $\Delta sipD$ strain exhibited a shorter needle (~45 nm) in comparison to the needle filaments of injectisomes from the wild-type or $\Delta sipB$ strains (~50 nm). These observations suggest that SipD is the only structural component of the tip complex (**Figure 1E**). To further explore this hypothesis, we examined by cryo-ET the injectisomes of minicells obtained from *S. Typhimurium* strains expressing FLAG-epitope-tagged versions of SipB, SipC, and SipD, after labeling with anti-FLAG antibodies (*Lara-Tejero and Galán, 2009*) (**Figure 1F–H, Figure 1—figure supplement 1**). Only injectisomes from minicells obtained from the strain expressing SipD-FLAG showed the antibodies bound to the needle tip (**Figure 1H, Figure 1—figure supplement 1D,I**). This observation is consistent with the notion that, prior to cell contact, SipD is the main, and most likely only component of the tip-complex (*Lara-Tejero and Galán, 2009*).

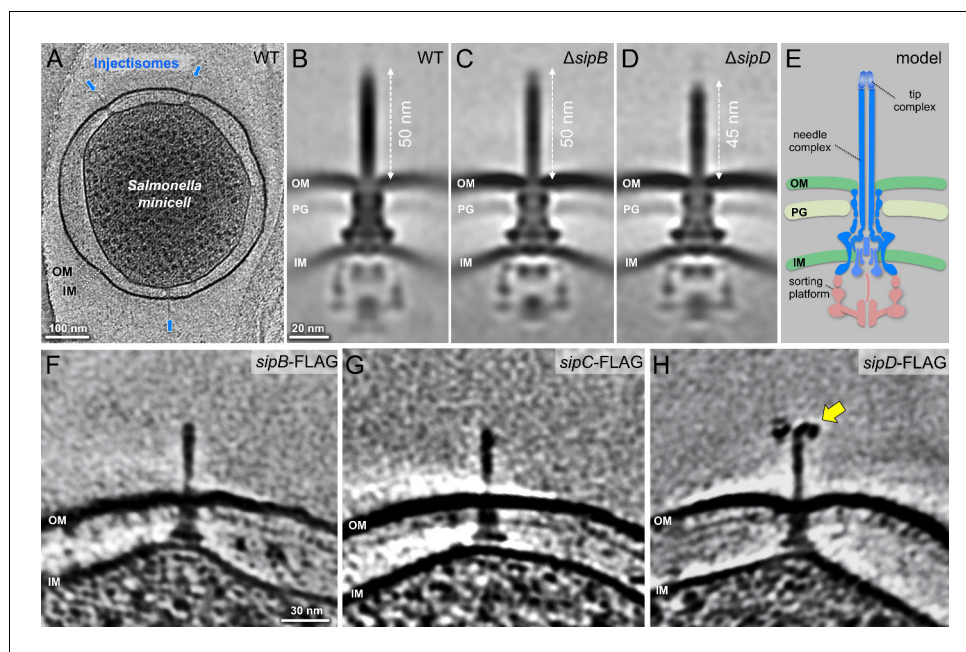


Figure 1. In situ structures of host-free *S. Typhimurium* T3SS injectisome in wild-type (WT), $\Delta sipB$, and $\Delta sipD$ minicells. (A) A central section of a tomogram showing *S. Typhimurium* minicell containing multiple injectisomes. (B–D) Central sections of sub-tomogram averages showing injectisomes of WT, $\Delta sipB$, and $\Delta sipD$, respectively. (E) A schematic of the injectisome. Outer membrane (OM), peptidoglycan (PG), sorting platform, and inner membrane (IM) of *S. Typhimurium* are annotated. (F–H) Central sections of tomograms showing injectisomes from strains expressing epitope-tagged (FLAG) SipB, SipC, and SipD, respectively. Yellow arrow indicates antibody bound to the epitope-tag.

DOI: <https://doi.org/10.7554/eLife.39514.002>

The following figure supplement is available for figure 1:

Figure supplement 1. Detection of FLAG-epitope-tagged SipB, SipC, and SipD Central slices from representative tomograms showing.

DOI: <https://doi.org/10.7554/eLife.39514.003>

High-resolution imaging of the T3SS mediated *Salmonella*-host cell interface

It is well established that effector translocation through the T3SS requires an intimate association between the bacteria and the host cell (Grosdent *et al.*, 2002). It has also been previously demonstrated that such intimate attachment requires an intact type III secretion machine, and in particular, the protein translocases, which most likely mediate such bacteria/host cell interaction (Lara-Tejero and Galán, 2009). Despite its central role in effector translocation, however, very little is known about the architecture of this specialized host/bacteria interface. This is largely because of

Table 1. Needle lengths of *S. Typhimurium* WT, $\Delta sipB$, $\Delta sipD$ and $\Delta sipBCD$ cells.

A summary of statistical measures including needle length average, standard deviation, and standard error of mean. Data were compared using an unpaired *t* test.

	Sample size	Average (nm)	Standard Deviation	Standard Error of Mean(nm)	P value compared to WT
WT	135	51.0	4.8	0.42	
$\Delta sipB$	46	50.6	4.0	0.59	0.62
$\Delta sipD$	61	46.5	3.9	0.50	<0.0001
$\Delta sipBCD$	46	45.3	3.0	0.44	<0.0001

DOI: <https://doi.org/10.7554/eLife.39514.004>

the lack of amenable experimental approaches that would allow a detail view of this interface. Cryo-ET is uniquely suited to examine host/pathogen interactions at high resolution. However, sample thickness limits the utility of this approach. To get around this limitation we used bacterial minicells as a surrogate for whole bacteria since it has been previously shown that they are capable of assembling functional T3SS injectisomes that can deliver de novo synthesized T3SS substrates into cultured cells (Carleton *et al.*, 2013). However, minicells are inefficient at triggering membrane ruffling, actin filament remodeling, and bacterial internalization due to inefficient partitioning of the effector proteins that trigger these responses. Consequently, while minicells are proficient at establishing a T3SS-mediated intimate association with cultured epithelial cells, they are inefficient at triggering their own internalization thus remaining firmly attached on the cell surface. These features make them ideally suited for high-resolution cryo-ET imaging. Therefore, we applied bacterial minicells obtained from wild-type *S. Typhimurium* onto cultured epithelial cells grown on cryo-EM grids. We found that the periphery of adherent cells is sufficiently thin (<500 nm) for high-resolution imaging (Figure 2—figure supplement 1). We readily observed T3SS injectisomes at the interface between minicells and the plasma membrane of cultured epithelial cells (Figure 2A,B). We found that in the presence of the injectisomes, the spacing between the surface of the *S. Typhimurium* minicells and the cultured-cell plasma membrane was ~50 nm, which matches the needle length of the injectisome imaged prior to their application to cultured cells (Figure 2—figure supplement 2A–F,M). The orientation of the injectisomes in the bacteria/target cell interface was perpendicular relative to the host PM, and the needle of the host-interacting injectisomes appeared straight (Figure 2C). We also observed that the interaction of the injectisome and the target cell resulted in a noticeable inward bend of the PM (Figure 2C, Video 1). Consistent with this observation, the distance between the bacterial cell and the PM was shorter (~30 nm) than the distance observed in areas immediately adjacent to the injectisomes (Figure 2—figure supplement 2A–L). However, we did not observe any sign of penetration of the needle filament through the host cell plasma membrane as it has been previously proposed (Hoiczuk and Blobel, 2001). The length of the bacterial-envelope-embedded injectisome base substructure before (30.5 ± 2.3 nm) and after (30.8 ± 2.2 nm) the bacteria/target cell interactions remained unchanged (Figure 2—figure supplement 2M,N). This is in contrast to the *Chlamydia* T3SS, which has been reported to undergo significant conformational changes upon contact with host cells (Nans *et al.*, 2015). The reasons for these differences are unclear and may either reflect intrinsic differences between these T3SS, or differences in the methodology used, which resulted in higher resolution of the visualized *S. Typhimurium* T3SS structures. Together, these observations indicate that (1) the interactions of the T3SS injectisome with the target cell results in the bending of the PM without penetration of the needle filament, and (2) upon contact with target cells the injectisome does not undergo conformational changes that could be seen at this level of resolution.

Visualization of the formation of the translocon in the target host cell membrane

The deployment of the translocon is an essential step in the T3SS-mediated delivery of effector proteins. However, very little information is available on both, the architecture of the assembled translocon, as well as the mechanisms leading to its deployment on the target cell. It is believed that the deployment process must be initiated by a sensing step most likely mediated by the tip complex (i.e. SipD), a step that must be followed by the subsequent secretion of the translocon components (i.e. SipB and SipC) destined to be inserted on the target eukaryotic cell PM. To capture the formation of the translocon, we analyzed over 600 injectisomes adjacent to the host PM. Classification of sub-tomograms depicting the region of the tip complex (Figure 3A) showed the PM at various conformations and distances to the needle tip (Figure 3B–I), which presumably represent intermediate steps prior to the deployment of the translocon and the resulting intimate attachment of the bacteria to the PM. After further alignment and classification of the injectisomes in intimate association with the PM, we obtained a distinct structure of the putative translocon in the host PM (Figure 3J). Sub-tomogram averages of injectisomes from the *S. Typhimurium* translocase-deficient mutants $\Delta sipB$ or $\Delta sipD$ in close proximity to the target cell PM did not show this distinct structure (Figure 3K,L), thus confirming that this density most likely corresponds to the assembled translocon. To better visualize the translocon in 3D, we segmented the distinct translocon structure in the context of the host PM, the needle, and its tip complex (Figure 3M,N). We found that the translocon

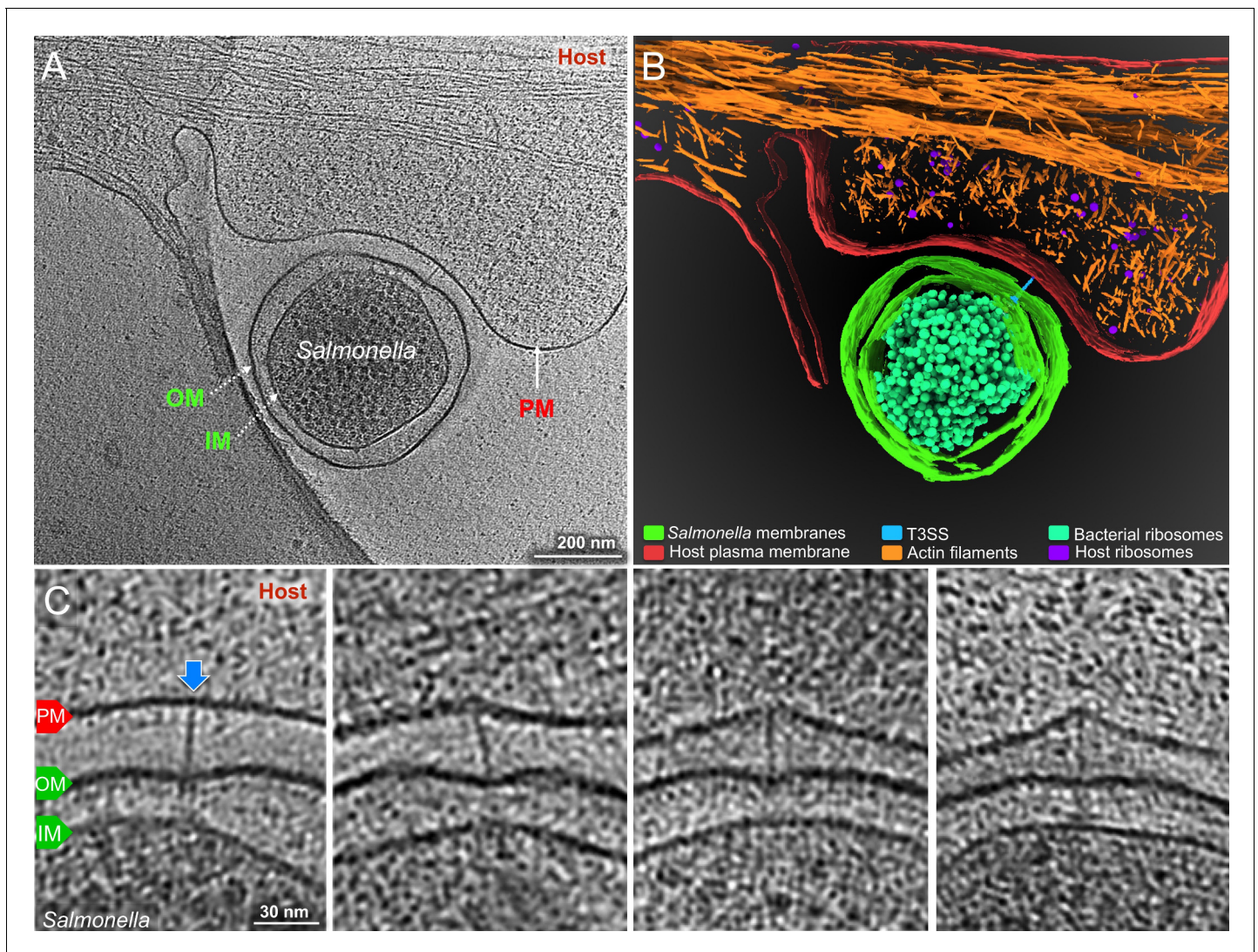


Figure 2. Visualization of the T3SS mediated *Salmonella*-Host interactions. (A) A central slice showing a *S. Typhimurium* minicell interacting with a host. Plasma membrane (PM) of HeLa cell, outer membrane (OM) and inner membrane (IM) of *S. Typhimurium* are annotated. (B) 3D rendering of the tomogram shown in (A). (C) Tomographic slices showing injectisomes interacting with the host PM. Blue arrows indicate needles attached to the host PM. Direction of the arrow represents the angle of needle perpendicular to the host PM.

DOI: <https://doi.org/10.7554/eLife.39514.005>

The following figure supplements are available for figure 2:

Figure supplement 1. Cultivation of mammalian cells (HeLa) on EM grid for cryo-ET.

DOI: <https://doi.org/10.7554/eLife.39514.006>

Figure supplement 2. Inter-membrane spacing between outer membrane and plasma membrane.

DOI: <https://doi.org/10.7554/eLife.39514.007>

has a thickness of 8.1 nm spanning the host PM and a diameter of 13.5 nm on its protruding portion (**Figure 3J**). This size is substantially smaller than reported size of the translocon of enteropathogenic *E. coli* assembled from purified proteins in vitro, which was estimated to be 55–65 nm in diameter (*Ide et al., 2001*). One half of the translocon is embedded in the host PM, while the other half protrudes towards the host cytoplasm. In the middle of the protruded portion, we observed a hemispherical hole, which may represent the channel through which effectors make their way into the target cell plasma membrane (**Figure 3N**). The presence of this structure is entirely consistent with the long-standing notion that the translocon forms a conduit through the host PM to facilitate the translocation of effectors (*Mueller et al., 2008*).



Video 1. A typical reconstruction shows the detailed interaction between the T3SS machines and the target cell and the membrane remodeling.

DOI: <https://doi.org/10.7554/eLife.39514.008>

target cell PM (Lara-Tejero and Galán, 2009). These data also further support the notion that the distinct structure embedded in host membrane in close apposition to the T3SS injectisome needle tip is formed by the translocon.

One of the striking features associated with the intimate T3SS mediated contact and the formation of the translocon is the target cell PM remodeling around the translocon-injectisome needle tip interface, appearing in a ‘tent-like’ conformation (Figure 2C, Video 1). This feature is likely the result of the close association between the bacteria and the target cell presumably mediated not only by the T3SS but also by multiple additional adhesins encoded by *S. Typhimurium*. In fact, the distance of the bacteria OM and the target cell is shorter than the length of the needle itself, which results in the bending of the target cell PM and the ‘tent-like’ conformation around the injectisome target cell PM interface. It is possible that this intimate association may facilitate the T3SS-mediated translocation of effector proteins (Figure 5, Video 2). These observations are also consistent with previous reports indicating that needle length, which presumably influences the ability of the bacteria to ‘push’ the needle against the host cell membrane, does contribute to type III secretion translocation efficiency (Mota et al., 2005).

Discussion

We have presented here a high-resolution view of the interface between the *S. Typhimurium* T3SS injectisome and the target eukaryotic cell plasma membrane, which has provided new details on the intimate attachment of this pathogen that precedes T3SS-mediated effector protein translocation. Notably, we observed a well-defined ‘bend’ on the target cell membrane in areas of the bacteria/host cell membrane interface surrounding the needle filament. These observations reflect the intimate attachment that is known to be required for optimal T3SS-mediated effector translocation. Importantly, we have been able to visualize a distinct density within the region of the target host cell membrane in close apposition to the needle tip of the T3SS injectisome. We present evidence that this density corresponds to the deployed T3SS translocon since this density was absent in the bacteria/PM interface of mutant bacteria that lack the translocon components. It has been previously shown that protein translocases SipB and SipC form a complex in the host membrane (Hayward and Koronakis, 1999; Myeni et al., 2013). Single-molecule fluorescence photobleaching experiments in a *Pseudomonas aeruginosa* T3SS further suggested that two translocases form a hetero-complex of defined stoichiometry in a membrane bilayer (Romano et al., 2016). Although our in situ structure of the translocon is not sufficient in detail to determine its stoichiometry, it appears to be large enough to accommodate multiple copies of SipB/SipC complex. The translocon is partially embedded in the host membrane. A large portion of the translocon extends towards the host cytoplasm, which is consistent with results in *P. aeruginosa* showing that the translocase PopB is stably inserted into lipid bilayers with its N-terminal domain and C-terminal ends exposed to the host cytoplasm (Discola et al., 2014). The dimensions of the in situ translocon structure determined in this study (~13.5 nm in diameter, 8 nm in thickness) are much smaller than previous estimates (50–65 nm in

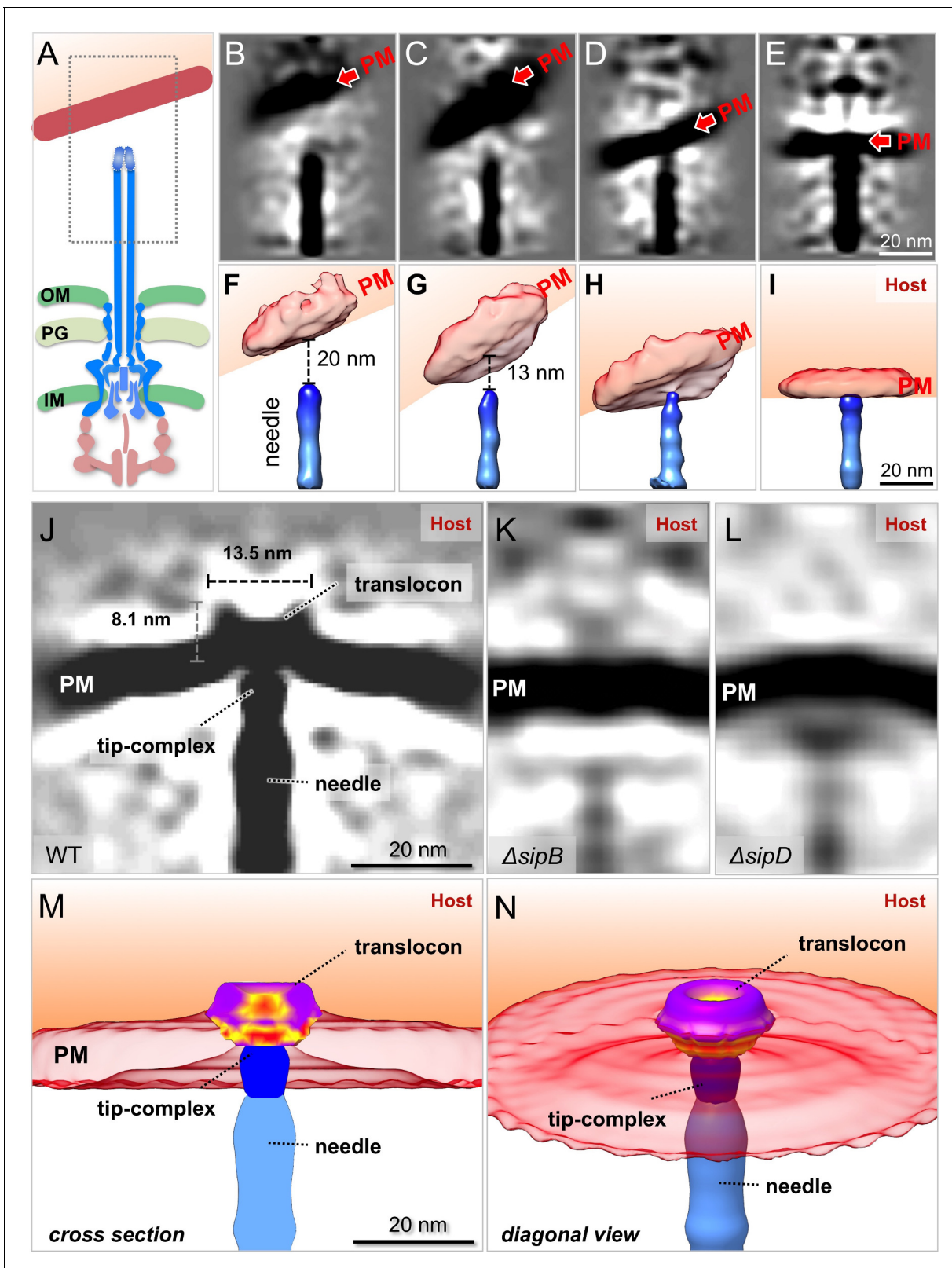


Figure 3. In situ structural analysis of the interface between the T3SS needle and the host membrane reveals a novel structure of the intact translocon. (A) A schematic representation of the *S. Typhimurium* injectisome with a box highlighting the area used for alignment and classification. (B–E) Central sections and (F–I) 3-D surface views of class averages showing different spacings between the needle and the plasma membrane (PM). (J–L) Central sections of WT, $\Delta sipB$, and $\Delta sipD$ strains, respectively. (M) 3-D surface view in cross-section and (N) 3-D surface view in diagonal view of the translocon, PM, tip-complex, and needle. Scale bars are 20 nm.

Figure 3 continued

sections of the sub-tomogram averages of the interface between the host PM and the needle of WT, $\Delta sipB$, and $\Delta sipD$, respectively. (M) Cross-section and (N) diagonal view of the surface rendering of the translocon in panel (J).

DOI: <https://doi.org/10.7554/eLife.39514.009>

diameter) obtained from the observation of EPEC translocons assembled from purified components on red blood cells (*Ide et al., 2001*). It is unlikely that these differences may reflect substantial differences between the dimensions of translocons from different T3SSs. It is possible that the observed differences may reflect differences in the experimental approaches used in the different studies. However, most likely these observations indicate fundamental differences in the translocon assembly mechanisms from purified components in comparison to translocon assembly during bacteria/target cell membrane interactions. It is well established that the deployment of the translocon during

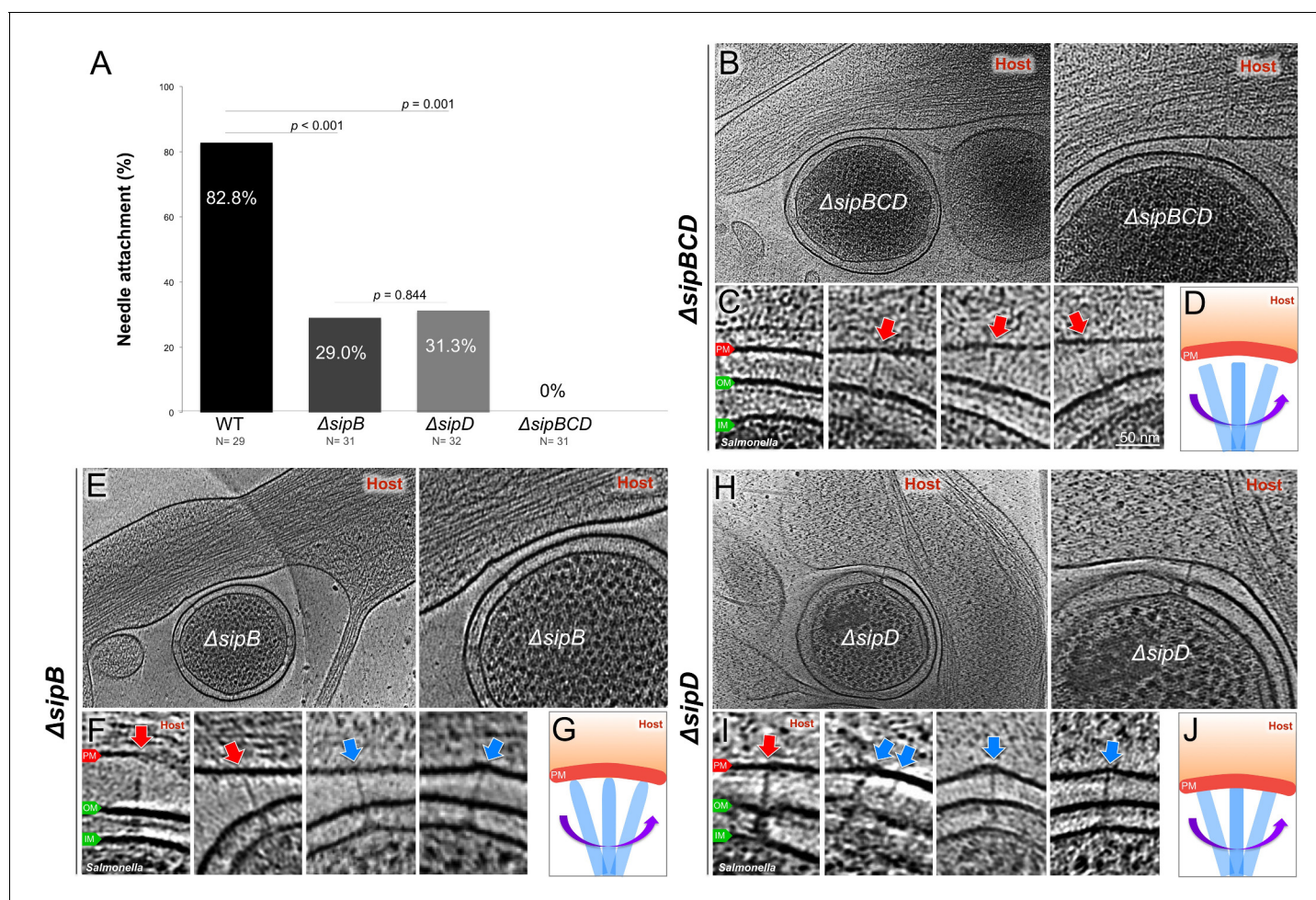


Figure 4. Deletion of the protein translocases disrupts the T3SS-dependent intimate attachment to the host PM, and the formation of the translocon. (A) Percentage of minicells attached to the host membrane via needle-membrane contact. Data were compared using a chi-squared test. (B, C) Central slices from tomograms showing the $\Delta sipBCD$ injectisomes interacting with the host PM. (E, F) Central slices from tomograms showing the $\Delta sipB$ injectisomes interacting with the host PM. (H, I) Central slices from tomograms showing the $\Delta sipD$ injectisomes interacting with the host PM. Blue arrows indicate needles attached to the host PM. Red arrows indicate unattached needles. (D, G, J) Schematic models depicting needle-attachment patterns from three mutants, respectively.

DOI: <https://doi.org/10.7554/eLife.39514.010>

The following figure supplement is available for figure 4:

Figure supplement 1. Gallery of snapshots from host-free and host-interacting *S. Typhimurium* minicells.

DOI: <https://doi.org/10.7554/eLife.39514.011>

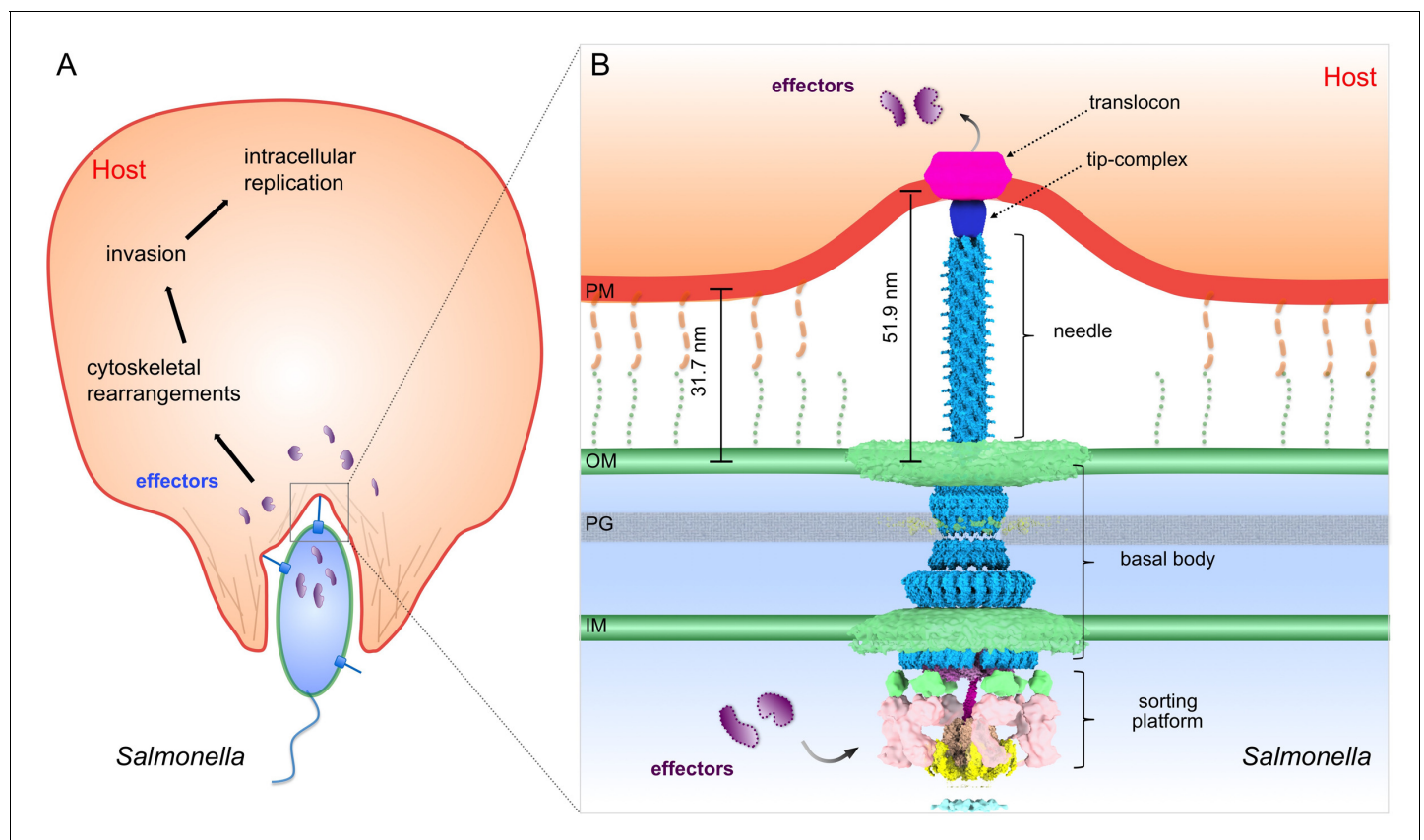


Figure 5. Model of the *S. Typhimurium* injectisome interacting with the host cell membrane. (A) A schematic diagram of *S. Typhimurium* interacting with the host cell. (B) Molecular model of the T3SS injectisome at the *Salmonella*-host cell interface.

DOI: <https://doi.org/10.7554/eLife.39514.012>

bacterial infections is orchestrated by the tip complex of the T3SS injectisome. In the absence of the tip protein, the components of the translocon are very efficiently secreted but they are unable to form the translocon (Kaniga *et al.*, 1995; Ménard *et al.*, 1994). It is therefore possible that the insertion in the membrane of the purified translocon components in the absence of the tip protein may lead to a structure that is substantially different from the one that results from the interaction of bacteria with target cells.

Contrary to what has been previously proposed for the *Chlamydia* T3SS (Nans *et al.*, 2015), we



Video 2. An animation shows the T3SS mediated *Salmonella*-host interaction and a plausible pathway of effector translocation.

DOI: <https://doi.org/10.7554/eLife.39514.013>

did not observe any obvious conformational changes in the injectisomes prior and post interaction with host cells. It is unlikely that these observations are an indication of fundamental differences between the T3SS injectisomes in different bacteria. Rather, the differences observed might reflect differences in the experimental approaches used in our studies, which resulted in a substantially higher resolution.

In summary, our studies have provided a close-up view of the interface between the T3SS injectisome and the target cell PM, which has resulted in the visualization of the deployed T3SS translocon complex. Importantly, given the highly conserved nature of the T3SSs among many Gram-negative bacteria, our studies have broad

scientific implications and provide a paradigm for the study of host-pathogen interactions in a greater detail.

Materials and methods

Key resources table

Reagent type (species) or resources	Designation	Source or reference	Identifiers	Additional information
Strain, strain background	SB1780 (<i>Salmonella enterica</i> serovar Typhimurium SL1344)	PMID: 23481398	<i>minD::cat</i> (wt)	Galán Laboratory (Yale University)
Strain, strain background	SB3542	This study	$\Delta sipB$ <i>minD::cat</i>	Galán Laboratory (Yale University)
Strain, strain background	SB3543	This study	$\Delta sipD$ <i>minD::cat</i>	Galán Laboratory (Yale University)
Strain, strain background	SB3141	This study	$\Delta sipBCD$ <i>minD::cat</i>	Galán Laboratory (Yale University)
Strain, strain background	SB3046	PMID: 28283062	$\Delta spaO$ <i>minD::cat</i>	Galán Laboratory (Yale University)
Strain, strain background	SB3544	This study	<i>sipB3xFLAG minD::cat</i>	Galán Laboratory (Yale University)
Strain, strain background	SB3545	This study	<i>sipB3xFLAG minD::cat</i>	Galán Laboratory (Yale University)
Strain, strain background	SB3546	This study	<i>sipB3xFLAG minD::cat</i>	Galán Laboratory (Yale University)
Genetic reagent	pSB3292 (Plasmid)	PMID: 28283062	<i>hila</i> in pBAD24	Galán Laboratory (Yale University)
Genetic reagent	<i>minD::cat</i> P22 (P22 bacteriophage lysate)	Galán Laboratory (Yale University)	P22 lysate from SB1780 S. Typhimurium strain	Source of <i>minD::cat</i> allele
Cell line	HeLa	ATCC	Hela (ATCC CCL-2)	
Antibody	M2	Sigma-Aldrich	F3165	1:1000 by volume
Chemical compound, drug	LB Broth	Fisher BioReagents	BP1426	
Chemical compound, drug	LB Agar	Fisher BioReagents	BP1425	
Chemical compound, drug	L-arabinose	VWR	1B1473	
Chemical compound, drug	Ampicillin Sodium Salt	Fisher BioReagents	BP1760-25	
Other	Gold grid	Quantifoil	R 2/1 on Au 200 mesh	
Software, algorithm	SerialEM	PMID: 16182563	http://bio3d.colorado.edu/SerialEM/	Data acquisition
Software, algorithm	MotionCor2	PMID: 28250466	http://msg.ucsf.edu/em/software/motioncor2.html	Motion correction
Software, algorithm	Tomoauto	PMID: 26863591	https://github.com/DustinMorado/tomoauto	Tomogram reconstruction
Software, algorithm	Tomo3D	PMID: 25528570	https://sites.google.com/site/3demimageprocessing/tomo3d	Tomogram reconstruction
Software, algorithm	IMOD	PMID: 8742726	http://bio3d.colorado.edu/imod/	Tomogram reconstruction
Software, algorithm	I3	PMID: 16973379	http://www.electrontomography.org/	Sub-tomogram averaging

Continued on next page

Continued

Reagent type (species) or resources	Designation	Source or reference	Identifiers	Additional information
Software, algorithm	UCSF Chimera	PMID: 15264254	http://www.cgl.ucsf.edu/chimera/	3D rendering
Software, algorithm	UCSF ChimeraX	PMID: 28710774	https://www.rbvi.ucsf.edu/chimerax/	3D rendering

Bacterial strains

The minicell producing *S. Typhimurium* $\Delta minD$, which is referred to in this study as wild-type, has been previously described ([Carleton et al., 2013](#); [Hu et al., 2017](#)). Mutations in the genes encoding the translocases ($\Delta sipB$, $\Delta sipC$) or tip complex ($\Delta sipD$) proteins were introduced into the $\Delta minD$ *S. Typhimurium* strain by allelic exchange as previously described ([Lara-Tejero et al., 2011](#)). The strains were listed in Key Resources Table.

Isolation of minicells

Minicell producing bacterial strains were grown overnight at 37°C in LB containing 0.3M NaCl. Fresh cultures were prepared from a 1:100 dilution of the overnight culture and then grown at 37°C to late log phase in the presence of ampicillin (200 µg/mL) and L-arabinose (0.1%) to induce the expression of regulatory protein HilA and thus increase the number of injectisomes partitioning to the minicells ([Carleton et al., 2013](#)). To enrich for minicells, the culture was centrifuged at 1000 x g for 5 min to remove bacterial cells, and the supernatant fraction was further centrifuged at 20,000 x g for 20 min to collect the minicells. The minicell pellet was resuspended in Dulbecco's Modified Eagles Medium (DMEM) prior to their application to cultured HeLa cells.

Antibody labeling

Minicells expressing 3xFLAG-epitope-tagged versions of SipB, SipC, and SipD were incubated with a saturating amount of anti-FLAG antibody (1:1000 by volume) for 30 min at room temperature. After incubation, minicells were pelleted and resuspended in a fresh LB broth containing ampicillin (200 µg/ml) for 3 times to remove unbound antibodies.

Table 2. Number of tomograms collected and analyzed.

	Number of tomograms collected
WT - HeLa	458
$\Delta sipB$ - HeLa	46
$\Delta sipD$ - HeLa	52
$\Delta sipBCD$ - HeLa	86
$\Delta spaO$ - HeLa	84
WT minicells	85
$\Delta sipB$ minicell	115
$\Delta sipD$ minicell	142
<i>sipB</i> -FLAG - HeLa	9
<i>sipC</i> -FLAG - HeLa	8
<i>sipD</i> -FLAG - HeLa	11
<i>sipB</i> -FLAG	5
<i>sipB</i> -FLAG	7
<i>sipB</i> -FLAG	13
Total	1051

DOI: <https://doi.org/10.7554/eLife.39514.014>

HeLa cell culture on EM grid and infection

HeLa cells were cultured in DMEM supplemented with 10% fetal bovine serum and gentamicin (50 µg/ml). The day before plating, gold EM grids with 2/1 Quantifoil were placed in glass bottom Mat-Tek dishes (facilitating fluorescence imaging and removal for cryo-preservation) and coated with 0.1 mg/ml poly-D-lysine overnight at 37°C. After rinsing the grids with sterile water, freshly trypsinized HeLa cells were plated on top of the pre-treated grids that were allowed to grow overnight at 37°C/5% CO₂. To infect HeLa cells with *S. Typhimurium* minicells, grids with adherent HeLa cells were removed from the culture dish and minicells were directly applied to the grids.

Vitrification and cryoEM sample preparation

At different time points after infection, the EM grids with HeLa cells and *S. Typhimurium* minicells were blotted with filter paper and vitrified in liquid ethane using a gravity-driven plunger apparatus as described (Hu et al., 2017; Hu et al., 2015).

Cryo-ET data collection and reconstruction

The frozen-hydrated specimens were imaged with 300kV electron microscopes. 713 tomograms were acquired from single-axis tilt series at $-6\ \mu\text{m}$ defocus with cumulative doses of $\sim 80\ \text{e}^-/\text{\AA}^2$ using Polara equipped with a field emission gun and a direct detection device (Gatan K2 Summit). 313 tomograms were acquired from single-axis tilt series at $\sim 1\ \mu\text{m}$ defocus with cumulative doses of $\sim 50\ \text{e}^-/\text{\AA}^2$ using Titan Krios equipped with a field emission gun, an energy filter, Volta phase plate, and a direct detection device (Gatan K2 Summit). The tomographic package SerialEM (Mastrorade, 2005) was utilized to collect 35 image stacks at a range of tilt angles between -51° and $+51^\circ$ for each data set. Each stack contained 10–15 images, which were first aligned using Motioncorr (Li et al., 2013) and were then assembled into the drift-corrected stacks by TOMOAUTO (Hu et al., 2015). The drift-corrected stacks were aligned and reconstructed by using marker-free alignment (Winkler and Taylor, 2006) or IMOD marker-dependent alignment (Kremer et al., 1996). In total, 1051 tomograms ($3,600 \times 3,600 \times 400$ pixels) were generated for detailed examination of the *Salmonella*-host interactions (Table 2). The softwares used in the study were listed in Key Resources Table.

Sub-tomogram analysis

Sub-tomogram analysis was accomplished as described previously (Hu et al., 2015) to analyze over 700 injectisomes extracted from 458 tomograms. Briefly, we first identified the injectisomes visually on each minicell. Two coordinates along the needle were used to estimate the initial orientation of each particle assembly. For initial analysis, $4 \times 4 \times 4$ binned sub-tomograms ($128 \times 128 \times 128$ voxels) of the intact injectisome were used for alignment and averaging by using the tomographic package I3 (Winkler and Taylor, 2006; Winkler et al., 2009). Then multivariate statistical analysis and hierarchical ascendant classification were used to analyze the needle tip complex (Winkler et al., 2009).

3-D visualization and molecular modeling

Outer membrane (OM) and inner membrane (IM) of *S. Typhimurium*, Plasma membrane (PM) of HeLa cells, actin filaments, and ribosomes were segmented using EMAN2 (Chen et al., 2017). UCSF Chimera (Pettersen et al., 2004) and UCSF ChimeraX (Goddard et al., 2018) were used to visualize the sub-tomogram average structures in 3-D and build atomic model of the T3SS injectisome. The atomic model was built as described briefly (Hu et al., 2017) except for the basal body, which we docked PDB-5TCR (Worrall et al., 2016) and PDB-3J1W (Bergeron et al., 2013). Video clips for the supplemental videos were generated using UCSF Chimera, UCSF Chimera X, and IMOD, and edited with iMovie.

Distance measurement and statistical analysis

IMOD (3dmod Graph) was used to measure lengths (in pixels) of various features. Each measurement was recorded in MS Excel for statistical analysis: Mean, standard deviation, standard error of mean, and Welch's t-test.

Acknowledgements

This work was supported by Grants AI030492 (to JEG) from the National Institute of Allergy and Infectious Diseases, and GM107629 from the National Institute of General Medicine (to JL).

Additional information

Funding

Funder	Grant reference number	Author
National Institute of Allergy and Infectious Diseases	AI030492	Jorge E Galán
National Institute of General Medical Sciences	GM107629	Jun Liu

The funders had no role in study design, data collection and interpretation, or the decision to submit the work for publication.

Author contributions

Donghyun Park, Data curation, Formal analysis, Validation, Investigation, Visualization, Writing—original draft; Maria Lara-Tejero, Data curation, Investigation, Methodology, Writing—original draft; M Neal Waxham, Wenwei Li, Bo Hu, Data curation, Investigation; Jorge E Galán, Conceptualization, Supervision, Investigation, Writing—original draft, Project administration, Writing—review and editing; Jun Liu, Conceptualization, Supervision, Investigation, Methodology, Writing—original draft, Project administration, Writing—review and editing

Author ORCIDs

Donghyun Park  <http://orcid.org/0000-0003-2048-6004>

Jorge E Galán  <http://orcid.org/0000-0002-6531-0355>

Jun Liu  <http://orcid.org/0000-0003-3108-6735>

Decision letter and Author response

Decision letter <https://doi.org/10.7554/eLife.39514.017>

Author response <https://doi.org/10.7554/eLife.39514.018>

Additional files

Supplementary files

- Transparent reporting form

DOI: <https://doi.org/10.7554/eLife.39514.015>

Data availability

All data generated or analysed during this study are included in the manuscript and supporting files.

References

- Barta ML**, Guragain M, Adam P, Dickenson NE, Patil M, Geisbrecht BV, Picking WL, Picking WD. 2012. Identification of the bile salt binding site on IpaD from *Shigella flexneri* and the influence of ligand binding on IpaD structure. *Proteins: Structure, Function, and Bioinformatics* **80**:935–945. DOI: <https://doi.org/10.1002/prot.23251>, PMID: 22423359
- Bergeron JR**, Worrall LJ, Sgourakis NG, DiMaio F, Pfuetschner RA, Felise HB, Vuckovic M, Yu AC, Miller SI, Baker D, Strynadka NC. 2013. A refined model of the prototypical *Salmonella* SPI-1 T3SS basal body reveals the molecular basis for its assembly. *PLoS Pathogens* **9**:e1003307. DOI: <https://doi.org/10.1371/journal.ppat.1003307>, PMID: 23633951
- Blocker AJ**, Deane JE, Veenendaal AK, Roversi P, Hodgkinson JL, Johnson S, Lea SM. 2008. What's the point of the type III secretion system needle? *PNAS* **105**:6507–6513. DOI: <https://doi.org/10.1073/pnas.0708344105>, PMID: 18458349

- Carleton HA**, Lara-Tejero M, Liu X, Galán JE. 2013. Engineering the type III secretion system in non-replicating bacterial minicells for antigen delivery. *Nature Communications* **4**:1590. DOI: <https://doi.org/10.1038/ncomms2594>, PMID: 23481398
- Chen M**, Dai W, Sun SY, Jonasch D, He CY, Schmid MF, Chiu W, Ludtke SJ. 2017. Convolutional neural networks for automated annotation of cellular cryo-electron tomograms. *Nature Methods* **14**:983–985. DOI: <https://doi.org/10.1038/nmeth.4405>, PMID: 28846087
- Cheung M**, Shen DK, Makino F, Kato T, Roehrich AD, Martinez-Argudo I, Walker ML, Murillo I, Liu X, Pain M, Brown J, Frazer G, Mantell J, Mina P, Todd T, Sessions RB, Namba K, Blocker AJ. 2015. Three-dimensional electron microscopy reconstruction and cysteine-mediated crosslinking provide a model of the type III secretion system needle tip complex. *Molecular Microbiology* **95**:31–50. DOI: <https://doi.org/10.1111/mmi.12843>, PMID: 25353930
- Collazo CM**, Galán JE. 1997. The invasion-associated type III system of *Salmonella typhimurium* directs the translocation of Sip proteins into the host cell. *Molecular Microbiology* **24**:747–756. DOI: <https://doi.org/10.1046/j.1365-2958.1997.3781740.x>, PMID: 9194702
- Deane JE**, Roversi P, Cordes FS, Johnson S, Kenjale R, Daniell S, Booy F, Picking WD, Picking WL, Blocker AJ, Lea SM. 2006. Molecular model of a type III secretion system needle: Implications for host-cell sensing. *PNAS* **103**:12529–12533. DOI: <https://doi.org/10.1073/pnas.0602689103>, PMID: 16888041
- Deng W**, Marshall NC, Rowland JL, McCoy JM, Worrall LJ, Santos AS, Strynadka NCJ, Finlay BB. 2017. Assembly, structure, function and regulation of type III secretion systems. *Nature Reviews Microbiology* **15**:323–337. DOI: <https://doi.org/10.1038/nrmicro.2017.20>, PMID: 28392566
- Dietsche T**, Tesfazgi Mebrhatu M, Brunner MJ, Abrusci P, Yan J, Franz-Wachtel M, Schärfe C, Zilkenat S, Grin I, Galán JE, Kohlbacher O, Lea S, Macek B, Marlovits TC, Robinson CV, Wagner S. 2016. Structural and functional characterization of the bacterial type III secretion export apparatus. *PLOS Pathogens* **12**:e1006071. DOI: <https://doi.org/10.1371/journal.ppat.1006071>, PMID: 27977800
- Discola KF**, Förster A, Boulay F, Simorre JP, Attree I, Dessen A, Job V. 2014. Membrane and chaperone recognition by the major translocator protein PopB of the type III secretion system of *Pseudomonas aeruginosa*. *Journal of Biological Chemistry* **289**:3591–3601. DOI: <https://doi.org/10.1074/jbc.M113.517920>, PMID: 24297169
- Galán JE**, Lara-Tejero M, Marlovits TC, Wagner S. 2014. Bacterial type III secretion systems: specialized nanomachines for protein delivery into target cells. *Annual Review of Microbiology* **68**:415–438. DOI: <https://doi.org/10.1146/annurev-micro-092412-155725>, PMID: 25002086
- Goddard TD**, Huang CC, Meng EC, Pettersen EF, Couch GS, Morris JH, Ferrin TE. 2018. UCSF ChimeraX: Meeting modern challenges in visualization and analysis. *Protein Science* **27**:14–25. DOI: <https://doi.org/10.1002/pro.3235>, PMID: 28710774
- Grosdent N**, Maridonneau-Parini I, Sory MP, Cornelis GR. 2002. Role of Yops and adhesins in resistance of *Yersinia enterocolitica* to phagocytosis. *Infection and Immunity* **70**:4165–4176. DOI: <https://doi.org/10.1128/IAI.70.8.4165-4176.2002>, PMID: 12117925
- Hayward RD**, Koronakis V. 1999. Direct nucleation and bundling of actin by the SipC protein of invasive *Salmonella*. *The EMBO Journal* **18**:4926–4934. DOI: <https://doi.org/10.1093/emboj/18.18.4926>, PMID: 10487745
- Hoiczky E**, Blobel G. 2001. Polymerization of a single protein of the pathogen *Yersinia enterocolitica* into needles punctures eukaryotic cells. *PNAS* **98**:4669–4674. DOI: <https://doi.org/10.1073/pnas.071065798>, PMID: 11287645
- Hu B**, Morado DR, Margolin W, Rohde JR, Arizmendi O, Picking WL, Picking WD, Liu J. 2015. Visualization of the type III secretion sorting platform of *Shigella flexneri*. *PNAS* **112**:1047–1052. DOI: <https://doi.org/10.1073/pnas.1411610112>, PMID: 25583506
- Hu B**, Lara-Tejero M, Kong Q, Galán JE, Liu J. 2017. In situ molecular architecture of the *Salmonella* type III secretion machine. *Cell* **168**:1065–1074. DOI: <https://doi.org/10.1016/j.cell.2017.02.022>, PMID: 28283062
- Ide T**, Laarmann S, Greune L, Schillers H, Oberleithner H, Schmidt MA. 2001. Characterization of translocation pores inserted into plasma membranes by type III-secreted Esp proteins of enteropathogenic *Escherichia coli*. *Cellular Microbiology* **3**:669–679. DOI: <https://doi.org/10.1046/j.1462-5822.2001.00146.x>, PMID: 11580752
- Kaniga K**, Trollinger D, Galán JE. 1995. Identification of two targets of the type III protein secretion system encoded by the *inv* and *spa* loci of *Salmonella typhimurium* that have homology to the *Shigella* IpaD and IpaA proteins. *Journal of Bacteriology* **177**:7078–7085. DOI: <https://doi.org/10.1128/jb.177.24.7078-7085.1995>, PMID: 8522512
- Kremer JR**, Mastronarde DN, McIntosh JR. 1996. Computer visualization of three-dimensional image data using IMOD. *Journal of Structural Biology* **116**:71–76. DOI: <https://doi.org/10.1006/jsbi.1996.0013>, PMID: 8742726
- Kubori T**, Matsushima Y, Nakamura D, Uralil J, Lara-Tejero M, Sukhan A, Galán JE, Aizawa SI. 1998. Supramolecular structure of the *Salmonella typhimurium* type III protein secretion system. *Science* **280**:602–605. DOI: <https://doi.org/10.1126/science.280.5363.602>, PMID: 9554854
- Lara-Tejero M**, Galán JE. 2009. *Salmonella enterica* serovar typhimurium pathogenicity island 1-encoded type III secretion system translocases mediate intimate attachment to nonphagocytic cells. *Infection and Immunity* **77**:2635–2642. DOI: <https://doi.org/10.1128/IAI.00077-09>, PMID: 19364837
- Lara-Tejero M**, Kato J, Wagner S, Liu X, Galán JE. 2011. A sorting platform determines the order of protein secretion in bacterial type III systems. *Science* **331**:1188–1191. DOI: <https://doi.org/10.1126/science.1201476>, PMID: 21292939

- Li X, Mooney P, Zheng S, Booth CR, Braunfeld MB, Gubbens S, Agard DA, Cheng Y. 2013. Electron counting and beam-induced motion correction enable near-atomic-resolution single-particle cryo-EM. *Nature Methods* **10**:584–590. DOI: <https://doi.org/10.1038/nmeth.2472>, PMID: 23644547
- Loquet A, Sgourakis NG, Gupta R, Giller K, Riedel D, Goosmann C, Griesinger C, Kolbe M, Baker D, Becker S, Lange A. 2012. Atomic model of the type III secretion system needle. *Nature* **486**:276–279. DOI: <https://doi.org/10.1038/nature11079>, PMID: 22699623
- Mastrorade DN. 2005. Automated electron microscope tomography using robust prediction of specimen movements. *Journal of Structural Biology* **152**:36–51. DOI: <https://doi.org/10.1016/j.jsb.2005.07.007>, PMID: 16182563
- Ménard R, Sansonetti P, Parsot C. 1994. The secretion of the *Shigella flexneri* Ipa invasins is activated by epithelial cells and controlled by IpaB and IpaD. *The EMBO Journal* **13**:5293–5302. DOI: <https://doi.org/10.1002/j.1460-2075.1994.tb06863.x>, PMID: 7957095
- Misselwitz B, Kreibich SK, Rout S, Stecher B, Periaswamy B, Hardt WD. 2011. *Salmonella enterica* serovar Typhimurium binds to HeLa cells via Fim-mediated reversible adhesion and irreversible type three secretion system 1-mediated docking. *Infection and Immunity* **79**:330–341. DOI: <https://doi.org/10.1128/IAI.00581-10>, PMID: 20974826
- Mota LJ, Journet L, Sorg I, Agrain C, Cornelis GR. 2005. Bacterial injectisomes: needle length does matter. *Science* **307**:1278. DOI: <https://doi.org/10.1126/science.1107679>, PMID: 15731447
- Mueller CA, Broz P, Cornelis GR. 2008. The type III secretion system tip complex and translocon. *Molecular Microbiology* **68**:1085–1095. DOI: <https://doi.org/10.1111/j.1365-2958.2008.06237.x>, PMID: 18430138
- Myeni SK, Wang L, Zhou D. 2013. SipB-SipC complex is essential for translocon formation. *PLoS One* **8**:e60499. DOI: <https://doi.org/10.1371/journal.pone.0060499>, PMID: 23544147
- Nans A, Kudryashev M, Saibil HR, Hayward RD. 2015. Structure of a bacterial type III secretion system in contact with a host membrane in situ. *Nature Communications* **6**:10114. DOI: <https://doi.org/10.1038/ncomms10114>, PMID: 26656452
- Notti RQ, Stebbins CE. 2016. The structure and function of type III secretion systems. *Microbiology Spectrum* **4**. DOI: <https://doi.org/10.1128/microbiolspec.VMBF-0004-2015>, PMID: 26999392
- Pettersen EF, Goddard TD, Huang CC, Couch GS, Greenblatt DM, Meng EC, Ferrin TE. 2004. UCSF Chimera—a visualization system for exploratory research and analysis. *Journal of Computational Chemistry* **25**:1605–1612. DOI: <https://doi.org/10.1002/jcc.20084>, PMID: 15264254
- Rathinavelan T, Lara-Tejero M, Lefebvre M, Chatterjee S, McShan AC, Guo DC, Tang C, Galán JE, De Guzman RN. 2014. NMR model of PrgI-SipD interaction and its implications in the needle-tip assembly of the *Salmonella* type III secretion system. *Journal of Molecular Biology* **426**:2958–2969. DOI: <https://doi.org/10.1016/j.jmb.2014.06.009>, PMID: 24951833
- Romano FB, Tang Y, Rossi KC, Monopoli KR, Ross JL, Heuck AP. 2016. Type 3 secretion translocators spontaneously assemble a hexadecameric transmembrane complex. *Journal of Biological Chemistry* **291**:6304–6315. DOI: <https://doi.org/10.1074/jbc.M115.681031>, PMID: 26786106
- Schraidt O, Lefebvre MD, Brunner MJ, Schmied WH, Schmidt A, Radics J, Mechtler K, Galán JE, Marlovits TC. 2010. Topology and organization of the *Salmonella typhimurium* type III secretion needle complex components. *PLoS Pathogens* **6**:e1000824. DOI: <https://doi.org/10.1371/journal.ppat.1000824>, PMID: 20368966
- Schraidt O, Marlovits TC. 2011. Three-dimensional model of *Salmonella*'s needle complex at subnanometer resolution. *Science* **331**:1192–1195. DOI: <https://doi.org/10.1126/science.1199358>, PMID: 21385715
- Winkler H, Taylor KA. 2006. Accurate marker-free alignment with simultaneous geometry determination and reconstruction of tilt series in electron tomography. *Ultramicroscopy* **106**:240–254. DOI: <https://doi.org/10.1016/j.ultramic.2005.07.007>, PMID: 16137829
- Winkler H, Zhu P, Liu J, Ye F, Roux KH, Taylor KA. 2009. Tomographic subvolume alignment and subvolume classification applied to myosin V and SIV envelope spikes. *Journal of Structural Biology* **165**:64–77. DOI: <https://doi.org/10.1016/j.jsb.2008.10.004>, PMID: 19032983
- Worrall LJ, Hong C, Vuckovic M, Deng W, Bergeron JR, Majewski DD, Huang RK, Spreter T, Finlay BB, Yu Z, Strynadka NC. 2016. Near-atomic-resolution cryo-EM analysis of the *Salmonella* T3S injectisome basal body. *Nature* **540**:597–601. DOI: <https://doi.org/10.1038/nature20576>, PMID: 27974800
- Zierler MK, Galán JE. 1995. Contact with cultured epithelial cells stimulates secretion of *Salmonella typhimurium* invasion protein InvJ. *Infection and Immunity* **63**:4024–4028. PMID: 7558314